Electronic Supplementary Information

Template-directed bifunctional NiS_x/nitrogen-doped mesoporous carbon electrocatalyst for rechargeable Zn–air batteries

Kai Wan[1], Jiangshui Luo[1,2,3]*, Xuan Zhang[1]*, Chen Zhou[1], Jin Won Seo[1], Palaniappan Subramanian[1], Jia-Wei Yan[3], Jan Fransaer[1]*

[1] Department of Materials Engineering, KU Leuven, Leuven 3001, Belgium.

[2] Collaborative Innovation Center of Clean Energy, Longyan University, Longyan 364012, China.

[3] State Key Laboratory of Physical Chemistry of Solid Surfaces and Department of Chemistry, College of Chemistry and Chemical Engineering, Xiamen University, Xiamen 361005, China.

*Corresponding author: E-mail: jiangshui.luo@gmail.com (J. Luo), xuan.zhang@kuleuven.be (X. Zhang), jan.fransaer@kuleuven.be (J. Fransaer).

1. Electrode preparation

1) Thin-film electrode for rotating disk electrode evaluations

The catalyst dispersion was prepared as follows: 5.0 mg of the catalyst was dispersed in 400 μL EtOH, 40 μL 5 wt. % Nafion (Nafion® DE 520, Sigma-Aldrich) and 60 μL deionized water by sonication for 30 min. Then 10 μL catalyst dispersion was transferred onto the glassy carbon disk by using a pipette and dried at room temperature. The catalyst loading on the electrode was 500 μg cm^{-2}. The catalyst loading of IrO_2 and 10 wt. % Pt/C are the same as the as-synthesized catalyst.

2) Air electrode for cell performance evaluation

The as-synthesized catalyst together with Nafion resin (Nafion® DE 520, Sigma-Aldrich) (mass ratio: 9:1), was dispersed in 2.0 mL ethanol and then sonicated for 30 min. Then 1 mg cm^{-2} catalyst was deposited onto a gas diffusion layer (PTFE wet-proofed carbon paper with 1 mg cm^{-2} Vulcan XC-72R) to fabricate the air electrode. Similarly, the 10 wt. % Pt/C + IrO_2 catalyst (mass ratio of Pt/C vs. IrO_2 1:1) was also used to prepare the air electrode with the same loading.

2. Calibration of reference electrode potentials

All potentials were calibrated to the RHE potential based on the Nernst equation:

$$E_{\mathrm{RHE}} = E^{\ominus}_{\mathrm{Hg/HgO}} + 0.0591\ \ V \times \mathrm{pH} \tag{1}$$

where $E^{\ominus}_{\mathrm{Hg/HgO}}$ is the standard electrode potential of the Hg/HgO electrode (0.098 V *vs.* SHE).

3. *IR*-corrections

All potentials were *IR*-corrected to compensate for the influence of electrolyte resistances, using the following equation:

$$E_{\text{IR-corrected}} = E - IR \tag{2}$$

Where I is the current and R is the uncompensated electrolyte ohmic resistance measured by electrochemical impedance spectroscopy (EIS).

4. Overpotential (η)

The overpotential (η) for OER is calculated using the following equation:

$$\eta = E_{\text{IR-corrected}} - 1.23\ \ V \tag{3}$$

5. Tafel slope

The Tafel slope is determined by fitting polarization data to the Tafel equation:

$$\eta = a + b * \log|j| \tag{4}$$

where η is the overpotential, b is the Tafel slope, and j is the current density.

6. Electron transfer number (n)

The kinetic current density (j_K) is extracted from the RDE results based on the Koutecky-Levich equation:

$$\frac{1}{j} = \frac{1}{j_K} + \frac{1}{j_L} = \frac{1}{j_K} + \frac{1}{B\omega^{1/2}} \tag{5}$$

$$B = 0.62n\mathrm{F}D^{2/3}\nu^{-1/6}C \tag{6}$$

where n is the electron transfer number, F is the Faraday constant (96485 C mol^{-1}), D is the diffusion coefficient of oxygen in 0.1 M KOH solution (1.9×10^{-9} m^2 s^{-1}), ν is the kinematic viscosity of 0.1 M KOH solution (1.0×10^{-6} m^2 s^{-1}), C is the saturated concentration of oxygen in 0.1 M KOH (1.1 mol m^{-3}), and ω is the angular rotation rate.

7. Discharge process of Zn-air battery in 1.0 M KOH

Anode:

$$\mathrm{Zn} \rightarrow \mathrm{Zn}^{2+} + 2\mathrm{e}^- \tag{7}$$

$$\mathrm{Zn}^{2+} + 4\mathrm{OH}^- \rightarrow \mathrm{Zn(OH)}_4^{2-} \tag{8}$$

$$\mathrm{Zn(OH)_4^{2-}(sol) \rightarrow ZnO(s) + H_2O + 2OH^-} \qquad E_0 = -1.25\ \mathrm{V} \tag{9}$$

Cathode:

$$\mathrm{O_2 + 2H_2O + 4e^- \rightarrow OH^-} \qquad E_0 = +0.40\ \mathrm{V} \tag{10}$$

8. Specific capacity and energy density for Zn-air batteries

The specific capacity was calculated using the equation below:

$$Q\ (\mathrm{Ah\ kg^{-1}}) = \frac{It}{\Delta m_{\mathrm{Zn}}} \tag{11}$$

The energy density was calculated *via* the equation below:

$$E\ (\mathrm{Wh\ kg^{-1}}) = \frac{VIt}{\Delta m_{\mathrm{Zn}}} \tag{12}$$

where I is the discharge current (A), t is the discharge time (h), V is the average discharge voltage (V), and Δm_{Zn} is the mass of zinc that is consumed (kg).

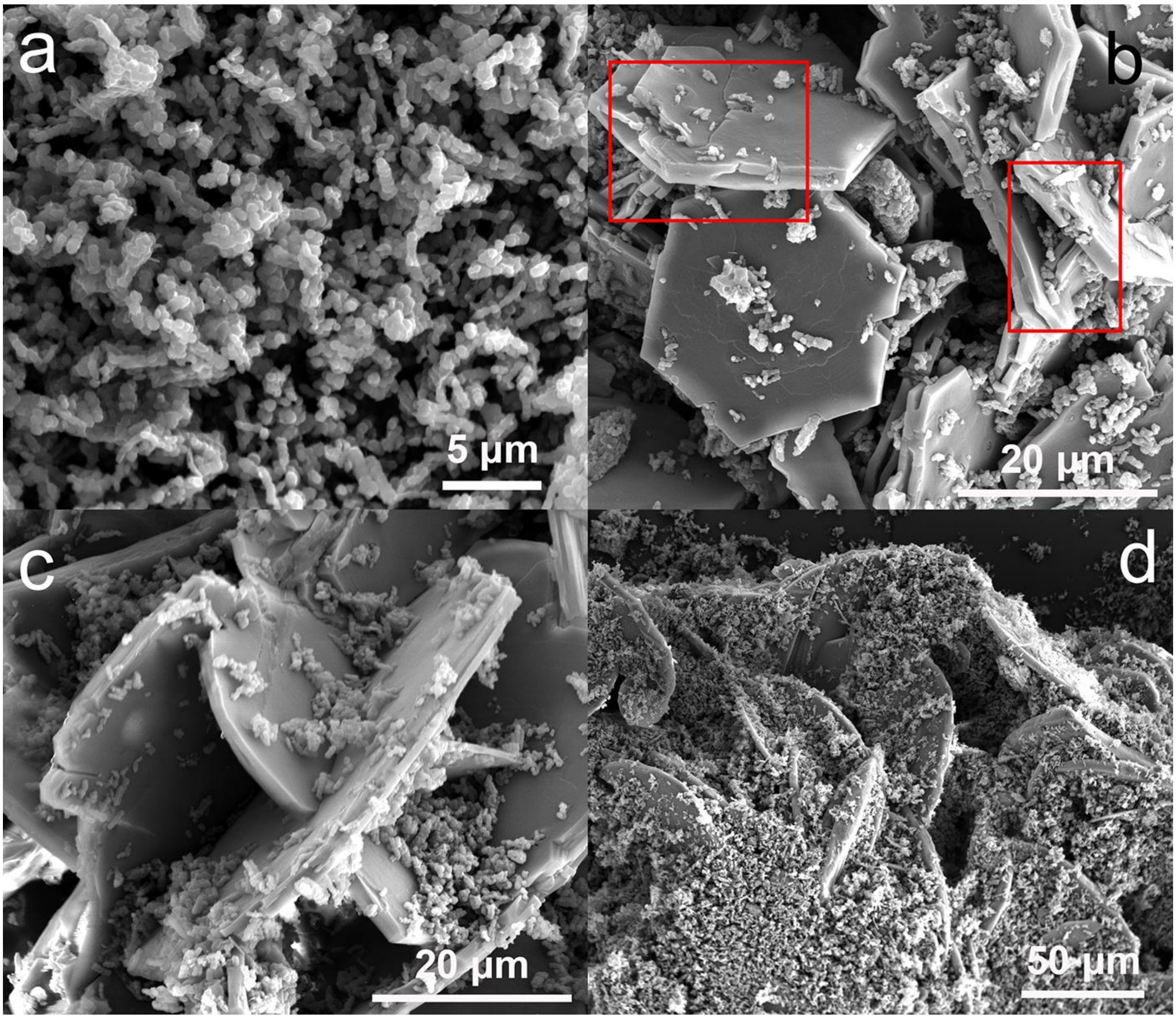

Fig. S1. SEM images: a) nitrogen-doped mesoporous carbon (NMC), b) Ni-MOF/NMC-0.5, c) Ni-MOF/NMC-1.5, d) Ni-MOF/NMC-3.0.

Scanning electron microscopy (SEM) images show that the NMC particles are distributed on the surface and inside the Ni-MOF structure (Fig. S1b). The Ni-MOFs were almost fully covered by the NMC particles when increasing the concentration of NMC from 0.5 mg mL^{-1} to 3.0 mg mL^{-1} (Fig. S1d).

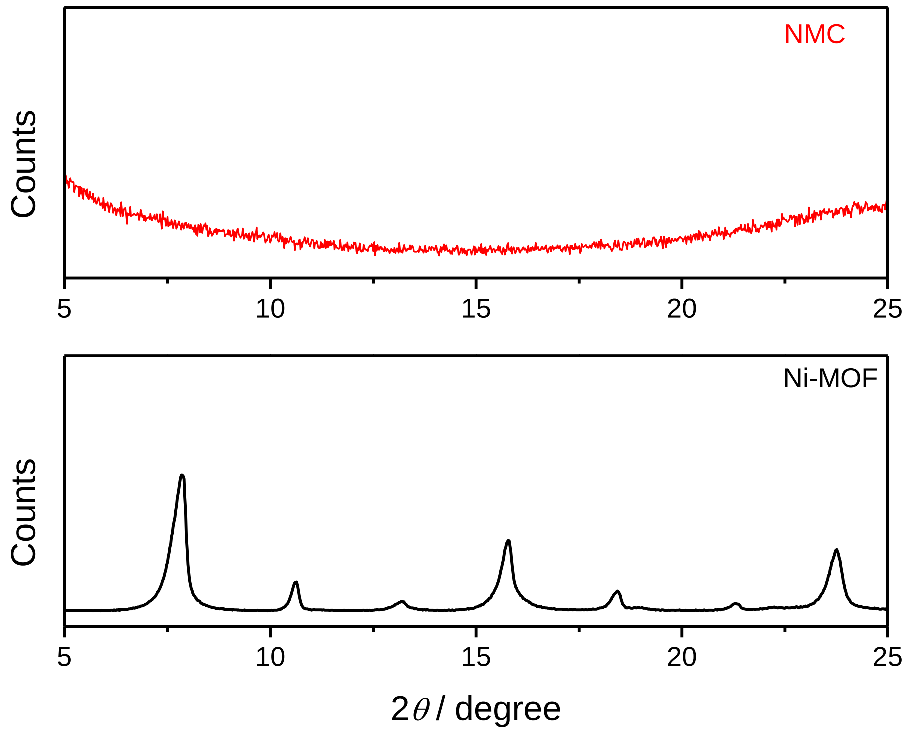

Fig. S2. XRD patterns of NMC (top) and Ni-MOF (bottom).

The 2θ diffraction peaks of 7.8°, 10.6°, 13.2°, 15.7°, 21.3° and 23.7° are in agreement with the simulation results.[1]

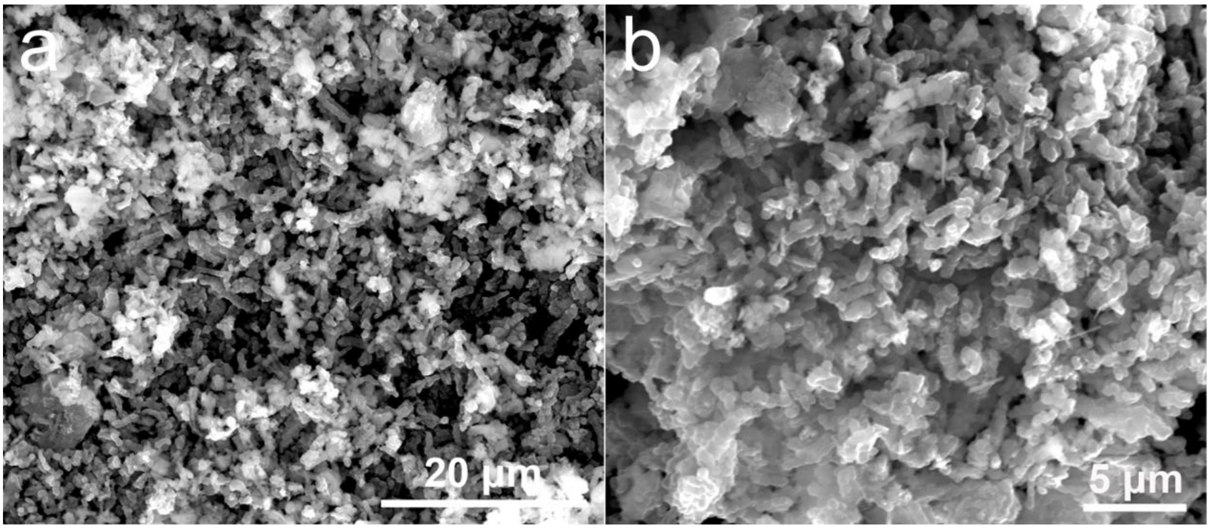

Fig. S3. SEM images of the NiS_x/NMC-1.5 catalyst.

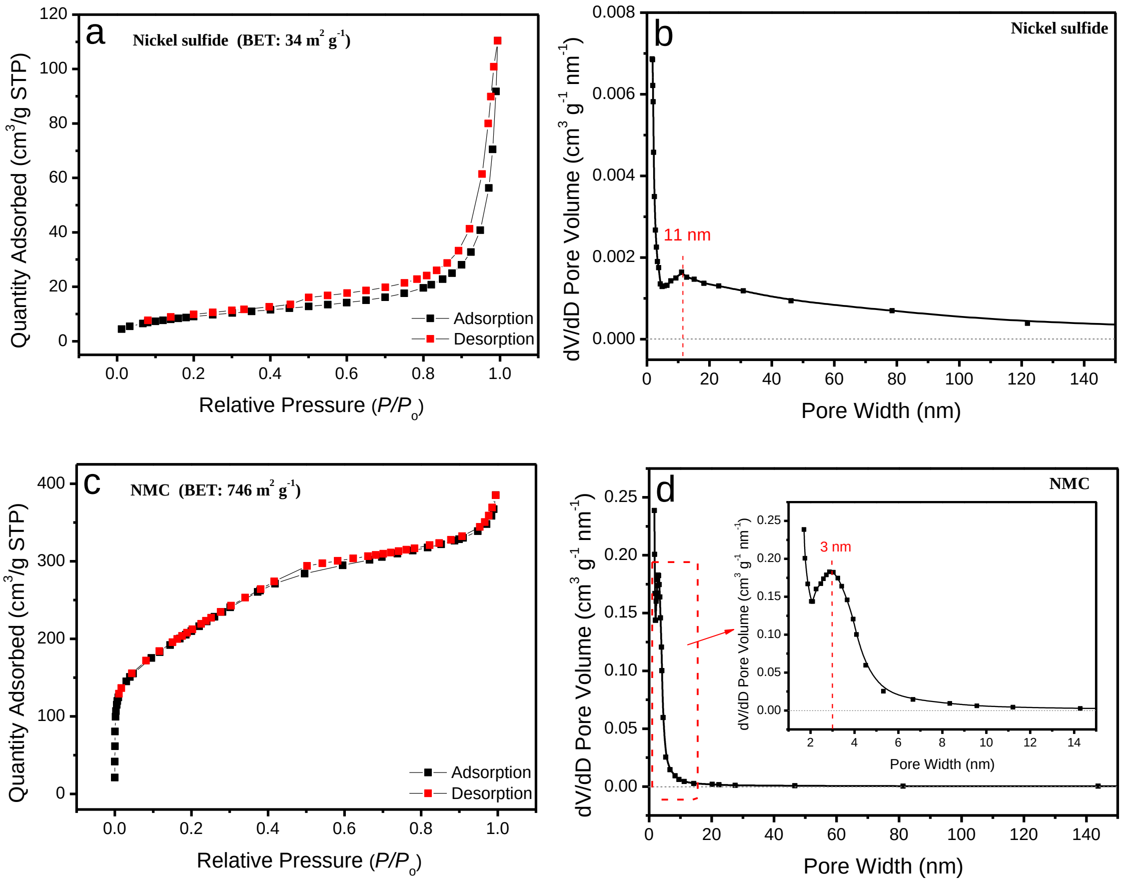

Fig. S4. Nitrogen adsorption/desorption isotherms and the corresponding pore volume distribution: a-b) Nickel sulfide, c-d) NMC.

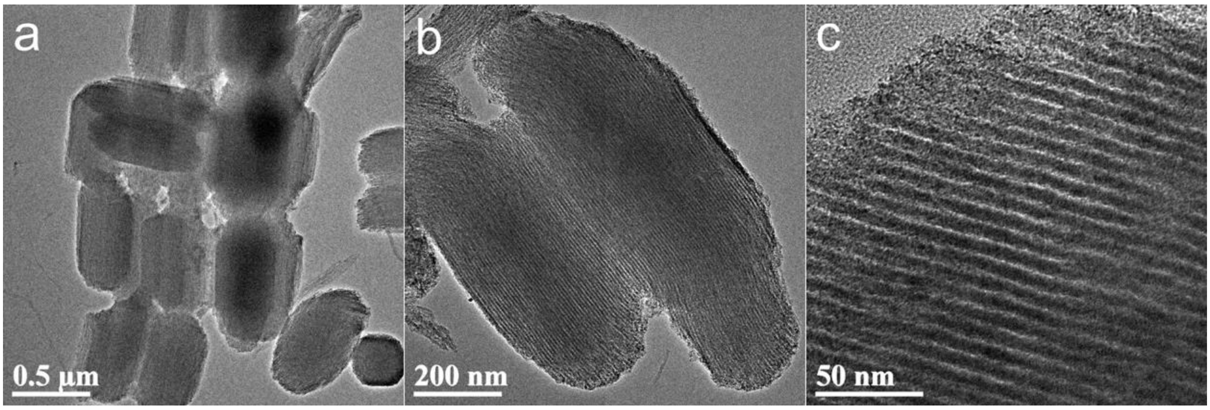

Fig. S5. TEM images of the NMC material.

The TEM images show that the NMC materials are necklace-like connected spherical particles with a highly ordered mesoporous structure.

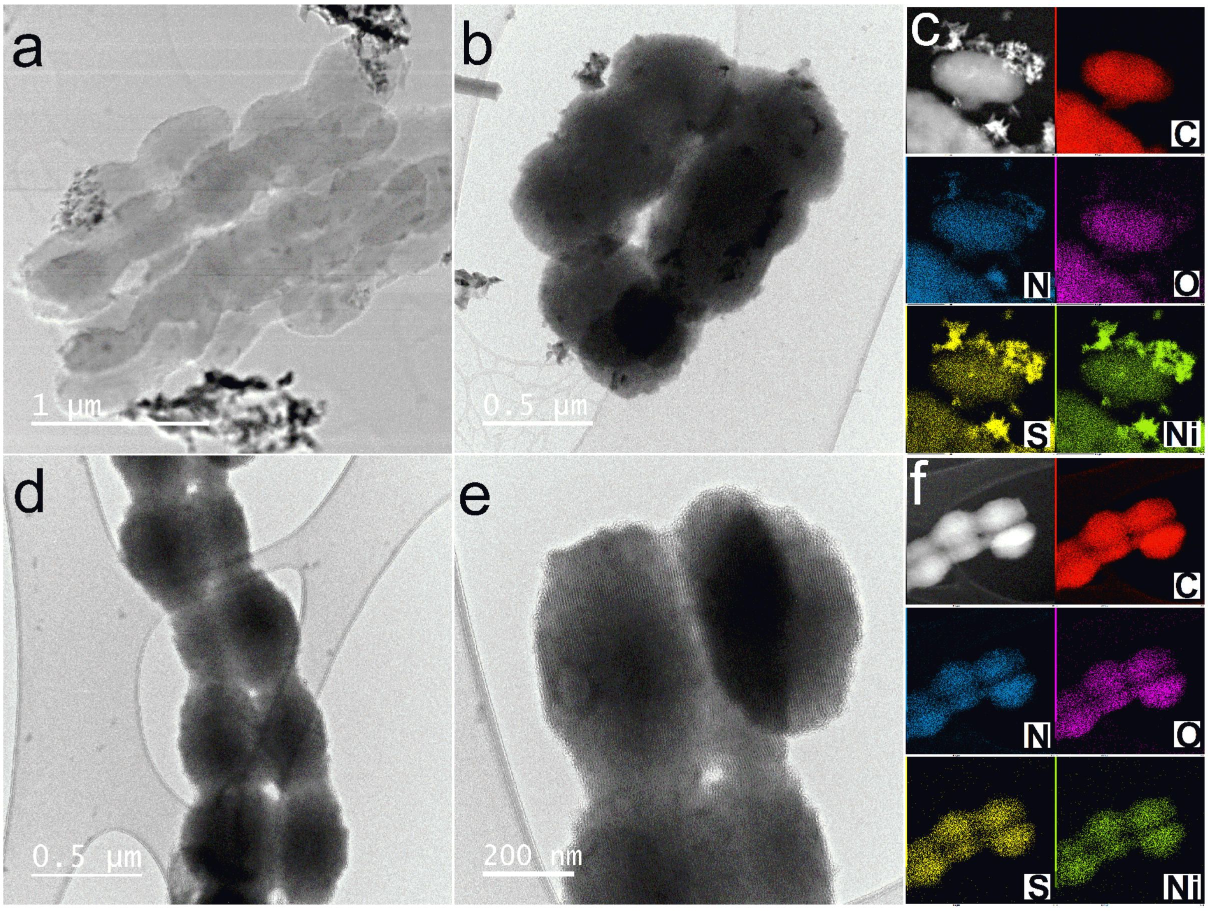

Fig. S6. TEM images and EDS mapping images: a-c) NiS_x/NMC-0.5; d-f) NiS_x/NMC-3.0.

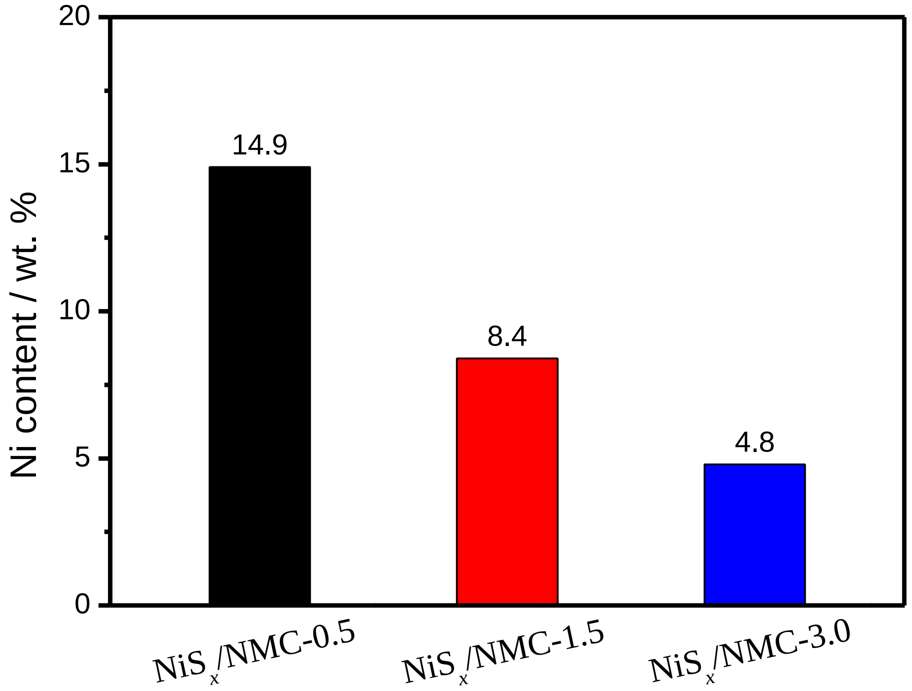

Fig. S7. Ni content (wt. %) of the NiS_x/NMC nanohybrids based on the ICP-OES measurements.

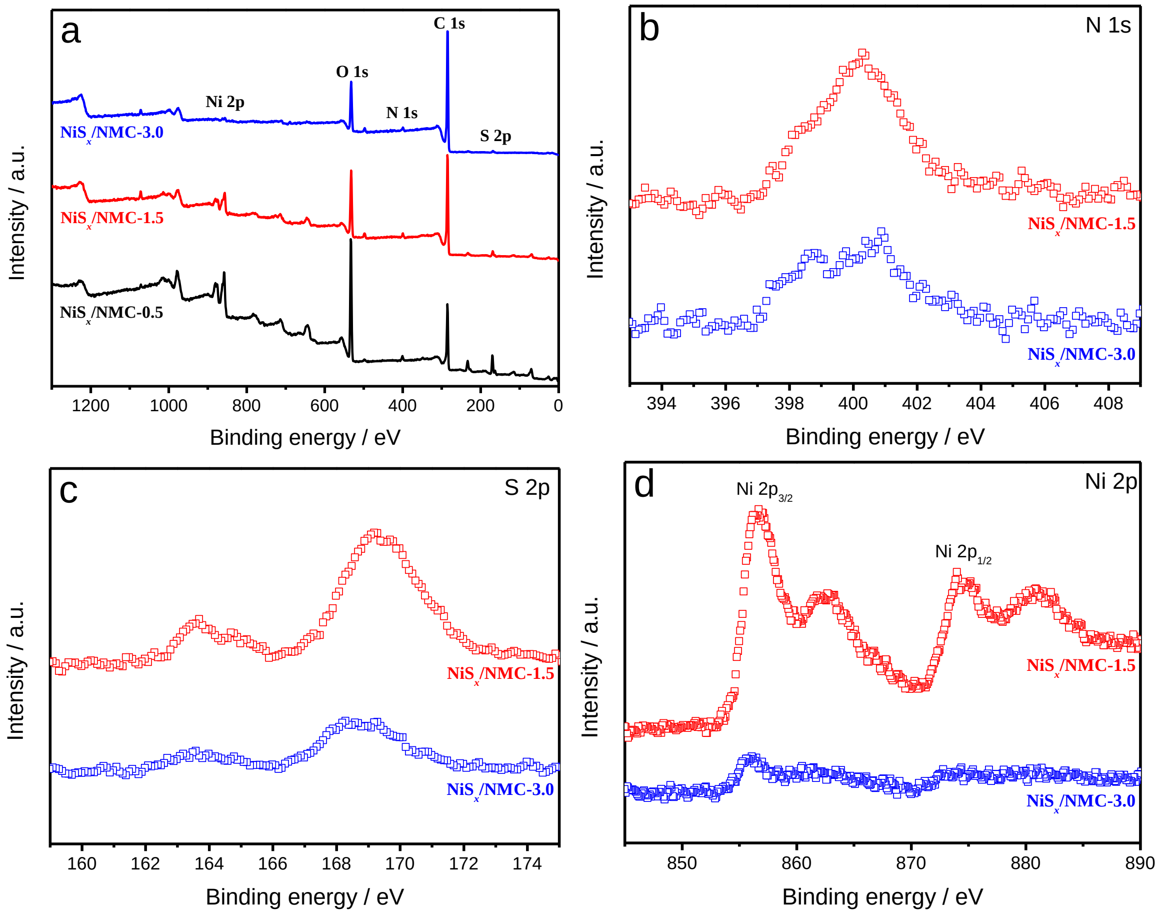

Fig. S8. a) XPS spectra of the NiS$_x$/NMC nanohybrids. b) N 1s peaks of the NiS$_x$/NMC-1.5 and NiS$_x$/NMC-3.0. c) S 2p peaks of the NiS$_x$/NMC-1.5 and NiS$_x$/NMC-3.0. d) Ni 2p peaks of the NiS$_x$/NMC-1.5 and NiS$_x$/NMC-3.0.

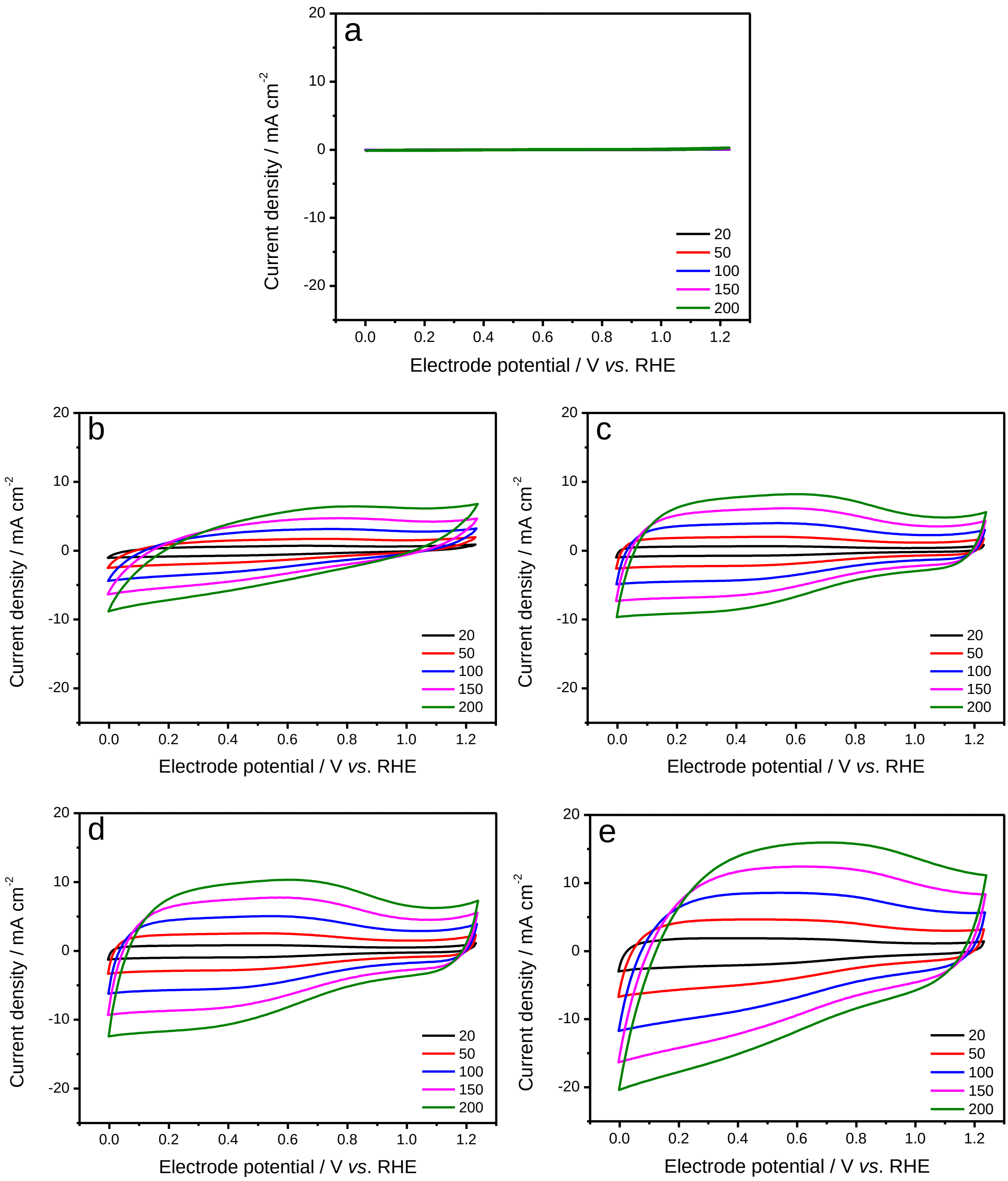

Fig. S9. Cyclic voltammograms of the as-prepared materials at various scan rates (mV s^{-1}) in Ar-saturated 0.1 M KOH: a) Nickel sulfide, b) NiS_x/NMC-0.5, c) NiS_x/NMC-1.5, d) NiS_x/NMC-3.0, e) NMC.

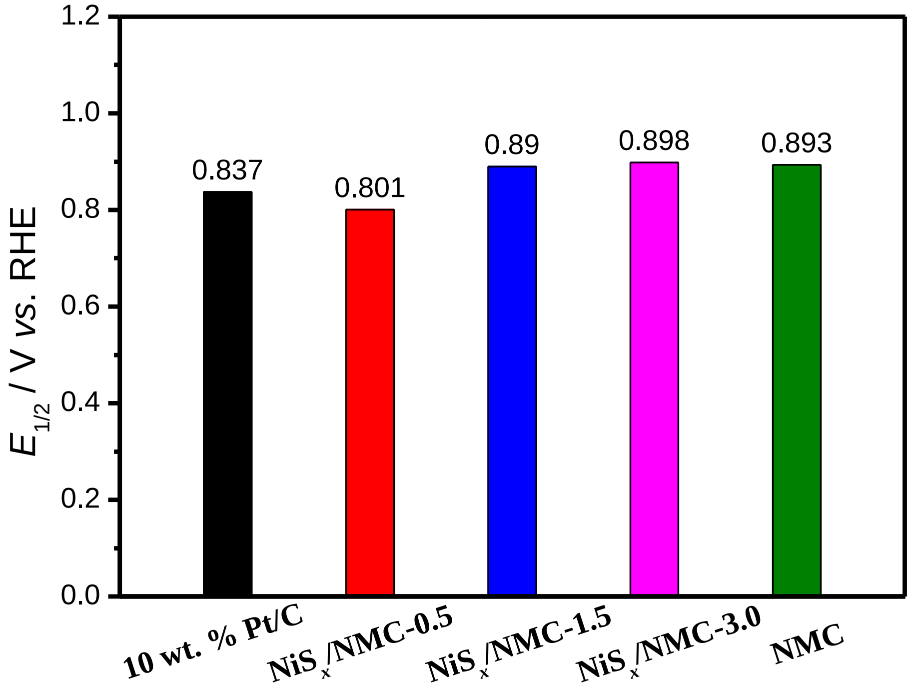

Fig. S10. The half-wave potentials ($E_{1/2}$) of ORR in O_2-saturated 0.1 M KOH catalyzed by the NiS$_x$/NMC nanohybrids and NMC catalysts *vs.* 10 wt. % Pt/C (extracted from the polarization curves shown in Fig. 4a).

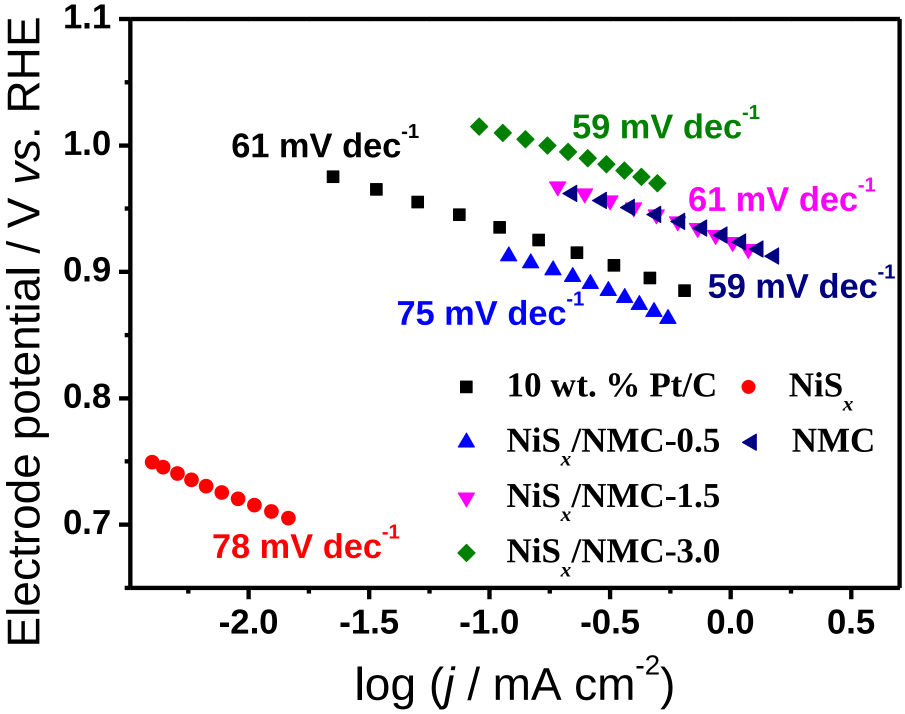

Fig. S11. . Tafel plot of the catalyst extracted from the ORR polarization curves shown in Fig. 4a.

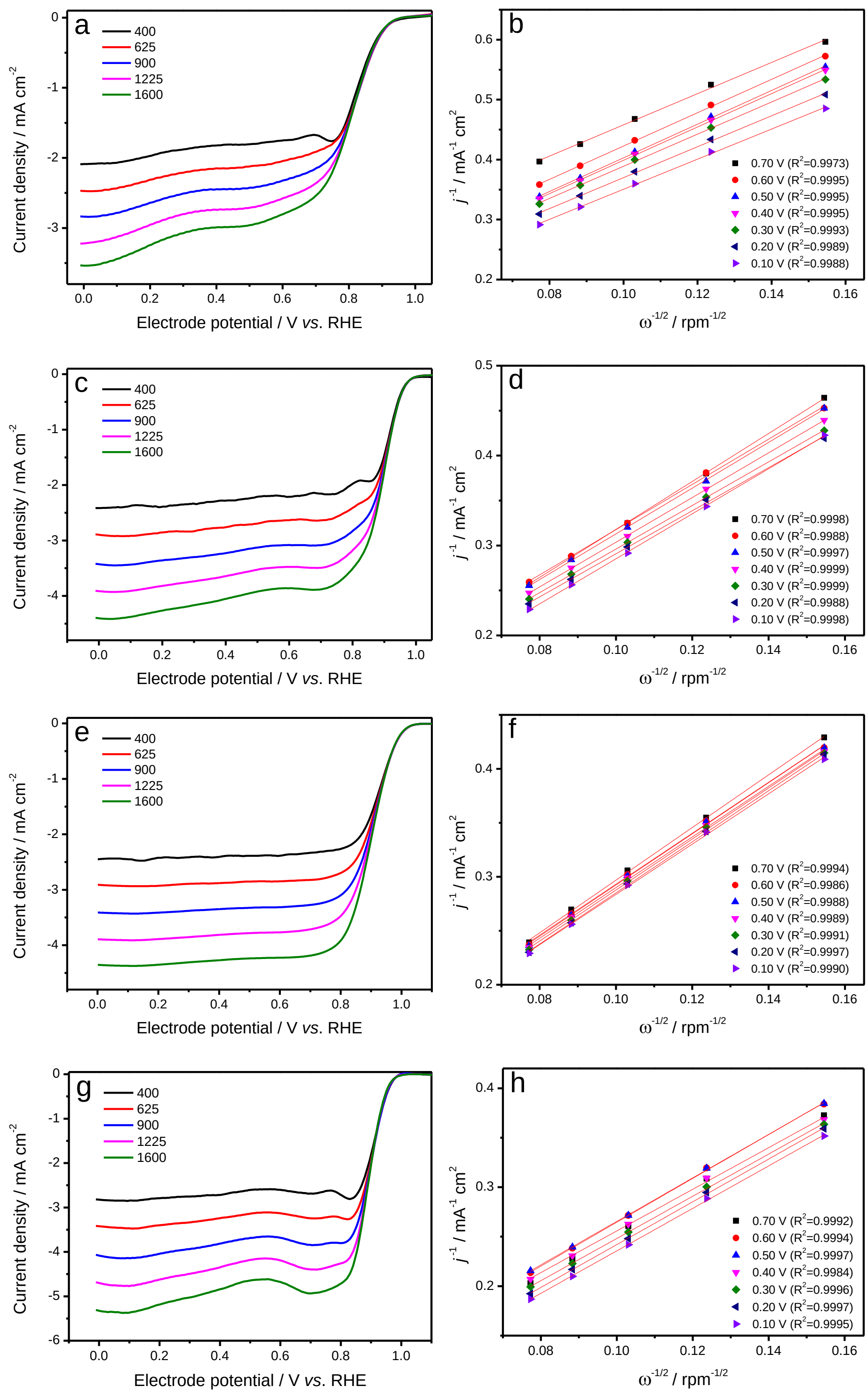

Fig. S12. The ORR polarization curves and corresponding Koutecky-Levich plots of the NiS_x/NMC nanohybrids and NMC at various rotating speeds in O_2-saturated 0.1 M KOH: a-b) NiS_x/NMC-0.5, c-d) NiS_x/NMC-1.5, e-f) NiS_x/NMC-3.0, g-h) NMC.

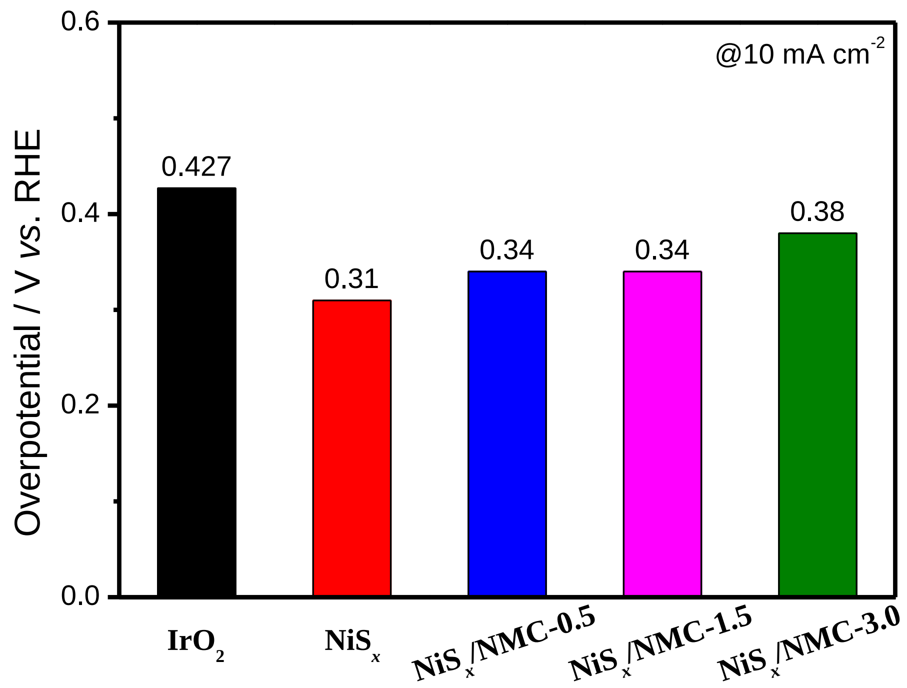

Fig. S13. The OER overpotentials at a current density of 10 mA cm^{-2} in 1.0 M KOH extracted from the polarization curves shown in Fig. 4c.

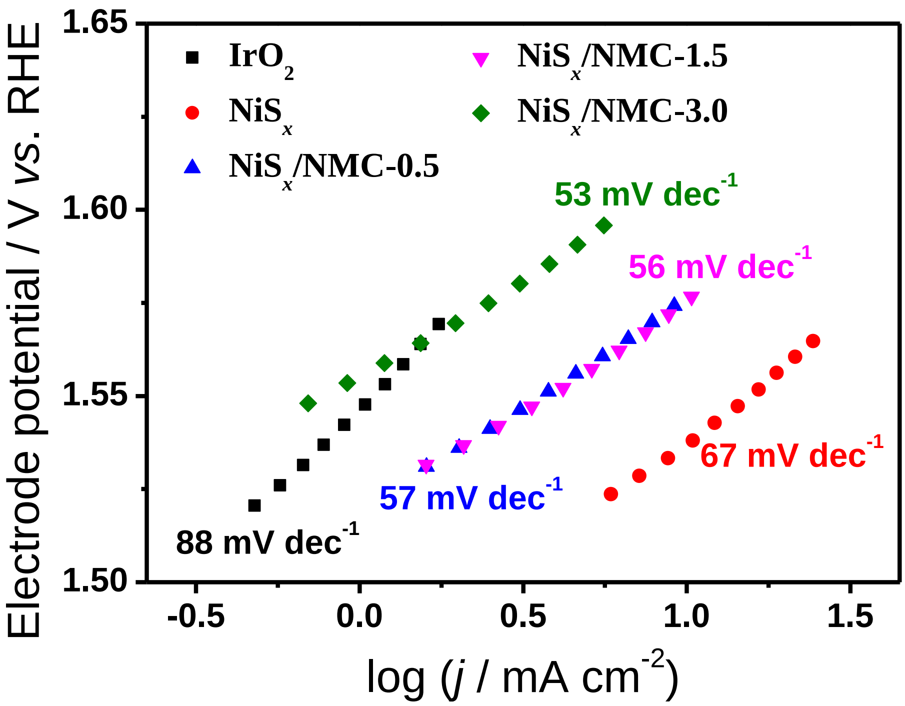

Fig. S14. Tafel plot of the catalyst extracted from the OER polarization curves shown in Fig. 4c.

Fig. S15. The photo of the Zn-air battery.

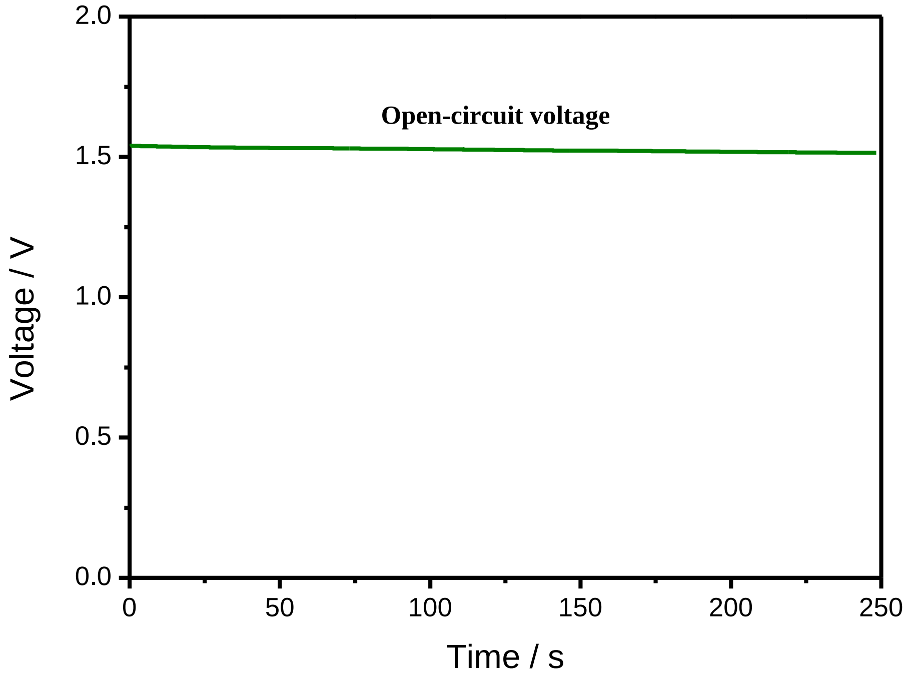

Fig. S16. Open-circuit voltage (OCV) of the Zn-air battery with NiS_x/NMC-1.5 as the catalyst for the air electrode.

1.5 electrode.

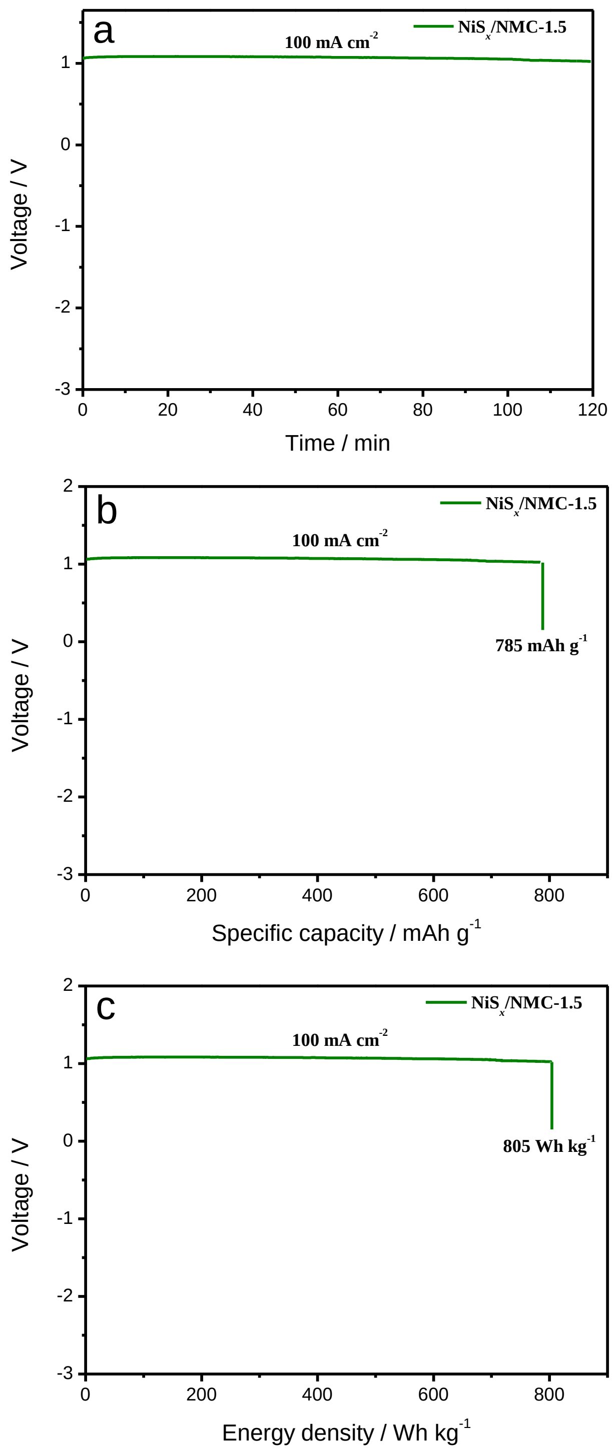

Fig. S17. a) Galvanostatic discharge at 100 mA cm^{-2} of the Zn-air battery with a NiS_x/NMC-1.5 electrode. b) Specific capacity and c) energy density of the Zn-air battery with a NiS_x/NMC-1.5 electrode.

Table S1. The ORR, OER and rechargeable Zn-air battery performances of the NiS_x/NMC-1.5 catalyst compared with those of metal-based bifunctional catalysts reported in literature.

Catalyst	**ORR & OER performance**				**Zn-air battery performance**						**Ref.**
	Catalyst loading / mg cm^{-2}	ORR $E_{1/2}$ / V	OER $E_{j=10}$ / V	ΔE / V	Electrolyte ORR OER	Catalyst loading /mg cm^{-2}	OCV / V	Peak power density / mW cm^{-2}	Specific capacity / mAh g^{-1}	Charge-discharge cycling	
NiS_x/NMC-1.5	0.5	0.89	1.57	0.68	0.1 M 1.0 M	1.0	1.53	186	785 @100 mA cm^{-2}	100 h @ 10 mA cm^{-2}	This work
CoP@SNC	0.6	0.79	1.580	0.790	0.1 M 1.0 M	-	1.45	-	-	30 @10 mA cm^{-2}	[2]
NiCo/NLG-270	0.4	0.820	1.570	0.750	0.1 M 1.0 M	0.8	1.49	103	403 @10 mA cm^{-2}	15 h [a]@2 mA cm^{-2} [b]@20 mA cm^{-2}	[3]
CoPi/NPGA	0.2	0.800	1.570	0.770	0.1 M 1.0 M	1.0	1.41	138	726 @15 mA cm^{-2}	40 h @15 mA cm^{-2}	[4]
Fe@C-NG/NCNTs	0.24	0.840	1.680	0.840	0.1 M 1.0 M	1.0	1.37	101	682 @10 mA cm^{-2}	99 h @10 mA cm^{-2}	[5]

CFZr(0.3)/N-rGO	0.4	0.730	1.570	0.840	0.1 M 1.0 M	2.0	1.39	-	732 @20 mA cm^{-2}	33 h @20 mA cm^{-2}	[6]
Meso/micro-FeCo-N_x-CN-30	0.1	0.886	1.670	0.784	0.1 M 1.0 M	2.0	1.41	150	-	40 @20 mA cm^{-2}	[7]
NC@Co-NGC DSNCs	0.4	0.82	1.64	0.82	0.1 M	0.5	1.45	109	537 @20 mA cm^{-2}	56 h @10 mA cm^{-2}	[8]
FeNi/NPC	0.485	0.730	1.490	0.760	0.1 M	1.0	-	-	800 @10 mA cm^{-2}	25 h @10 mA cm^{-2}	[9]
$NiCo_2O_4$/Co,N-CNTs NCs	0.5	0.862	1.569	0.707	0.1 M	1.0	1.45	174	-	45 h @5 mA cm^{-2}	[10]
CoNi/BCF	0.6	0.800	1.600	0.800	0.1 M	2.0	1.44	155	711 @10 mA cm^{-2}	30 h @10 mA cm^{-2}	[11]
CoZn-NC-700	0.24	0.840	1.620	0.78	0.1 M	1.2	1.42	152	578 @10 mA cm^{-2}	64 h @10 mA cm^{-2}	[12]
Fe/Co-N/S-Cs	0.35	0.832	1.515	0.683	0.1 M	1.0	1.40	103	-	26.7 h @5 mA cm^{-2}	[13]
FeNi-NC	0.24	0.830	1.640	0.810	0.1 M	1.0	-	81	-	23 h @8 mA cm^{-2}	[14]

Co_3O_4/NPGC	0.2	0.840	1.680	0.840	0.1 M	0.9	-	-	-	80 h @5 mA cm^{-2}	[15]
Co@NCNT HMS	0.28	0.866	1.547	0.681	1.0 M	1.0	1.48	160	676 @5 mA cm^{-2}	150 h @5 mA cm^{-2}	[16]
(Mg, Co)$_3O_4$@NGC	0.3	0.842	1.576	0.734	0.1 M	1.0	1.45	125	-	200 @10 mA cm^{-2}	[17]
$CuCo_2O_4$/N-CNTs	0.2	0.802	1.702	0.900	0.1 M	2.0	1.36	84	817 @100 mA cm^{-2}	48 h @20 mA cm^{-2}	[18]
$Fe_{0.5}Ni_{0.5}$@N-GR	0.2	0.830	1.440	0.610	0.1 M	2.0	1.48	85	765 @5 mA cm^{-2}	40 h @20 mA cm^{-2}	[19]
FeN_x/C-700-20	0.5	0.900	2.000	1.100	0.1 M	2.0	1.60	36	-	84 h @5 mA cm^{-2}	[20]
$Co_3FeS_{1.5}(OH)_6$	0.25	0.721	1.588	0.867	0.1 M	0.5	-	113	898 @20 mA cm^{-2}	36 @2 mA cm^{-2}	[21]

$\Delta E = E_{j=10} - E_{1/2}$, wherein $E_{j=10}$ refers to OER potential at 10 mA cm^{-2}, and $E_{1/2}$ refers to half-wave potential of ORR.

[a] charge current density

[b] discharge current density

References

[1] Y. Li, L. Xie, Y. Liu, R. Yang, X. Li, Inorg. Chem. (47) 2008 10372-10377.

[2] T. Meng, Y. N. Hao, L. Zheng, M. Cao, Nanoscale (10) 2018 14613-14626.

[3] X. R. Wang, J. Y. Liu, Z. W. Liu, W. C. Wang, J. Luo, X. P. Han, X. W. Du, S. Z. Qiao, J. Yang, Adv. Mater. (30) 2018 1800005.

[4] J. T. Ren, G. G. Yuan, L. Chen, C. C. Weng, Z. Y. Yuan, ACS Sustain. Chem. Eng. (6) 2018 9793-9803.

[5] Q. Wang, Y. Lei, Z. Chen, N. Wu, Y. Wang, B. Wang, Y. Wang, J. Mater. Chem. A (6) 2018 516-526.

[6] V. Kashyap, S. Kurungot, ACS Catal. (8) 2018 3715-3726.

[7] S. Li, C. Cheng, X. Zhao, J. Schmidt, A. Thomas, Angew. Chem. Int. Edit. (57) 2018 1856-1862.

[8] S. Liu, Z. Wang, S. Zhou, F. Yu, M. Yu, C. Y. Chiang, W. Zhou, J. Zhao, J. Qiu, Adv. Mater. (29) 2017 1700874.

[9] H. X. Zhong, J. Wang, Q. Zhang, F. Meng, D. Bao, T. Liu, X. Y. Yang, Z. W. Chang, J. M. Yan, X. B. Zhang, Adv. Sustain. Syst. (1) 2017 1700020.

[10] J. Li, S. Lu, H. Huang, D. Liu, Z. Zhuang, C. Zhong, ACS Sustain. Chem. Eng. (6) 2018 10021-10029.

[11] W. Wan, X. Liu, H. Li, X. Peng, D. Xi, J. Luo, Appl. Catal. B Environ. (240) 2019 193-200.

[12] B. Chen, X. He, F. Yin, H. Wang, D. J. Liu, R. Shi, J. Chen, H. Yin, Adv. Funct. Mater. (27) 2017 1700795.

[13]C. Li, H. Liu, Z. Yu, Appl. Catal. B Environ. (241) 2019 95-103.

[14]L. Yang, X. Zeng, D. Wang, D. Cao, Energy Storage Mater. (12) 2018 277-283.

[15]G. Li, X. Wang, J. Fu, J. Li, M. G. Park, Y. Zhang, G. Lui, Z. Chen, Angew. Chem. Int. Edit. (55) 2016 4977-4982.

[16]Y. Li, J. Gao, F. Zhang, Q. Qian, Y. Liu, G. Zhang, J. Mater. Chem. A (6) 2018 15523-15529.

[17]Y. P. Deng, Y. Jiang, D. Luo, J. Fu, R. Liang, S. Cheng, Z. Bai, Y. Liu, W. Lei, L. Yang, Z. Jing, C. Zhongwei, ACS Energy Lett. (2) 2017 2706-2712.

[18]H. Cheng, M. L. Li, C. Y. Su, N. Li, Z. Q. Liu, Adv. Funct. Mater. (27) 2017 1701833.

[19]P. Liu, D. Gao, W. Xiao, L. Ma, K. Sun, P. Xi, D. Xue, J. Wang, Adv. Funct. Mater. (28) 2018 1706928.

[20]S. Han, X. Hu, J. Wang, X. Fang, Y. Zhu, Adv. Energy Mater. (8) 2018 1800955.

[21]H. F. Wang, C. Tang, B. Wang, B. Q. Li, Q. Zhang, Adv. Mater. (29) 2017 1702327.